Structural and Magnetotransport Transitions in the Electron-Doped $Pr_{1-x}Sr_xMnO_3$ ($0.85 \leq x \leq 1$) Manganites

M. Hervieu,*,† C. Martin,† A. Maignan,† G. Van Tendeloo,‡ Z. Jirak,§ J. Hejtmanek,§ A. Barnabé,† D. Thopart,† and B. Raveau†

Laboratoire CRISMAT, UMR 6508 Associée au CNRS, ISMRA et Université de Caen, 6, Boulevard du Maréchal Juin, 14050 Caen Cedex, France; EMAT, University of Antwerp (RUCA), Groenenborgerlaan 171, B-2020, Antwerp, Belgium; and Institute of Physics of ASCR, Cukrovarnicka 10, 16253 Prague 6, Czech Republic

Received January 6, 2000. Revised Manuscript Received March 8, 2000

The exploration of the Mn^{4+}-rich side of the $Pr_{1-x}Sr_xMnO_3$ system has allowed the extension of the domain of the cubic perovskite, by using a two-step process, combining synthesis under Ar flow at high temperature and O_2 pressure annealing at lower temperature. We show that these Pr-doped cubic perovskites exhibit a coupled structural (cubic-tetragonal) and magnetic (para-antiferro) transition connected with a resistivity jump at the same temperature. The strong interplay between lattice, charges, and spins for these oxides results from the appearance at low temperature of the distorted C-type antiferromagnetic structure. The $Pr_{1-x}Sr_xMnO_3$ magnetic phase diagram shows, for $0.9 \leq x < 1$ (i.e., on the Mn^{4+}-rich side), the existence at low temperature of C- and G-type antiferromagnetism. The absence of ferromagnetic−antiferromagnetic competition explains that magnetoresistante properties are not observed in this system, in contrast to Mn^{4+}-rich $Ln_{1-x}Ca_xMnO_3$ systems.

Introduction

In the course of the recent investigations of the colossal magnetoresistant (CMR) manganites with the perovskite structure, very strong interplay between structural transitions and magnetotransport properties has been evidenced. This is the case of the Mn^{4+}-rich compounds $Ln_{1-x}Ca_xMnO_3$ with $x > 0.5$ which exhibit coupled structural (orthorhombic to monoclinic) and magnetic (paramagnetic (PM) to C-type antiferromagnetic (AFM)) transitions for $x \sim 0.80$. Close to this value ($x > 0.80$), irrespective the kind of lanthanide, the main distorted C-type phase coexists with pseudocubic regions which assume G-type antiferromagnetic order with appreciable ferromagnetic (FM) component, as reported for $Sm_{0.15}Ca_{0.85}MnO_3$.[1,2] The growth of this minority phase in applied magnetic field is the source of CMR properties in these systems. In contrast, for the $Ln_{1-x}Sr_xMnO_3$ strontium-rich phases ($0.85 \geq x > 0.5$), no CMR properties were found although a coupled structural and magnetic transition to this C-type phase was observed as shown for $Pr_{0.15}Sr_{0.85}MnO_3$.[2,3] It raised the question whether CMR properties could be achieved for richer Sr phases ($x > 0.90$); but unfortunately these compositions were found to be oxygen-deficient in our usual synthesis conditions in air and contain an hexagonal form of the perovskite as impurity.[3−5] The existence of oxygen nonstoichiometry was indeed shown for the first time by Negas and Roth[6] for $SrMnO_{3-\delta}$ ($x = 1$). These authors evidenced a wide range of oxygen deficiency, with $0 \leq \delta \leq 0.38$, and the appearance for $\delta = 0$ of a four-layer (4L) hexagonal structure, whereas for $\delta \cong 0.26-0.38$ a cubic metastable form was observed. As a consequence, the magnetic and transport properties of the $SrMnO_{3-\delta}$ perovskites are complex, depending on the structural symmetry and on the oxygen deficiency.[7−11] This great complexity of the $SrMnO_{3-\delta}$ perovskite suggests thus that the Sr-rich side of the $Pr_{1-x}Sr_xMnO_3$ system may also exhibit oxygen nonstoichiometry.

In the present paper, we show the possibility to stabilize Sr-rich cubic perovskites ($SrMnO_{2.92}$, $Pr_{0.05}Sr_{0.95}MnO_{2.92}$, and $Pr_{0.10}Sr_{0.90}MnO_3$) using a two-step method of synthesis and working under argon flow and oxygen pressure, successively. The magnetic and transport properties of these Pr-doped manganites reveal the existence of coupled magnetic and transport transitions, combined with a structural transition from cubic to tetragonal symmetry as T decreases, but no evidence

* Corresponding author. Fax: +33 2 31 95 16 00. E-mail: maryvonne.hervieu@ismra.fr.
† ISMRA et Université de Caen.
‡ University of Antwerp.
§ Institute of Physics of ASCR.

(1) Martin, C.; Maignan, A.; Damay, F.; Hervieu, M.; Raveau, B. *J. Solid State Commun.* **1997**, *102*, 551.
(2) Martin, C.; Maignan, A.; Hervieu, M.; Raveau, B.; Jirak, Z.; Kurbakov, A.; Trounov, V.; André, G.; Bourée, F. *J. Magn. Magn. Mater.* **1999**, *205*, 184.
(3) Martin, C.; Maignan, A.; Hervieu, M.; Raveau, B. *Phys. Rev. B* **1999**, *60*, 12191.
(4) Kikuchi, K.; Chiba, H.; Kikuchi, M.; Syono, Y. *J. Solid State Chem.* **1999**, *146*, 1.
(5) Wadsley, A. D. *Non stoichiometric compounds*; Mandelcorn, L., Ed.; Academic Press Inc.: New York, 1964.
(6) Negas, T.; Roth, R. S. *J. Solid State Chem.* **1970**, *1*, 409.
(7) Takeda, T.; Ohara, S. *J. Phys. Soc. Jpn.* **1974**, *37*, 275.
(8) Battle, P. O.; Gibb, T. C.; Jones, C. W. *J. Solid State Chem.* **1988**, *74*, 60.
(9) Jonker, G. H.; Van Santen, J. H. *Physica* **1950**, *16*, 337.
(10) MacChesney, J. B.; Williams, H. J.; Potter, J. F.; Sherwood, R. C. *Phys. Rev.* **1967**, *164*, 779.
(11) Lee, K. J.; Iguchi, E. *J. Solid State Chem.* **1995**, *114*, 242.

10.1021/cm000016o CCC: $19.00
Published on Web 04/18/2000

for CMR in contrast to the $Ln_{1-x}Ca_xMnO_3$ oxides ($0.80 < x \leq 0.90$).[12] The magnetic phase diagram on the Mn^{4+}-rich side of the system $Pr_{1-x}Sr_xMnO_3$ previously investigated[3] is completed.

Experimental Section

The $Pr_{1-x}Sr_xMnO_3$ samples were prepared following the standard ceramic process in air. Stoichiometric mixtures of Pr_6O_{11}, $SrCO_3$, and MnO_2 were heated at 1000 °C for 12 h, until complete decarbonation. The powders were then pressed in the form of bars, heated at 1200 °C for 12 h and finally sintered at 1500 °C for 12 h. The temperature was slowly decreased (5 deg min^{-1}) down to 800 °C and finally, the samples were quenched to room temperature. These air-synthesized samples are labeled "air".

In a second step, the "air" samples were then heated in argon flow at 1500 °C for 12 h and slowly cooled to room temperature (labeled "air+Ar").

In a last step, the "air+Ar" samples were annealed at 600 °C for 12 h under oxygen pressure (100 bar). These samples are labeled "air+Ar+O_2".

After decarbonation at 1000 °C, a $Pr_{0.1}Sr_{0.9}MnO_{3-\delta}$ sample was also directly synthesized in argon flow, in two steps (12 h at 1200 °C and 12 h at 1500 °C) with a slow cooling to room temperature (labeled "Ar").

The electron diffraction (ED) study at room temperature was carried out with a JEOL 200CX electron microscope fitted with a tilting-rotating sample holder (tilt ± 60°). The ED study versus temperature and the bright/dark field imaging was carried out with a JEOL 2010 electron microscope fitted with a double tilt cooling sample holder (±40° for 92 K $\leq T \leq$ 300 K). The ED patterns were recorded versus T, keeping a constant electron current density. The high-resolution electron microscopy (HREM) study was made with a TOPCON 002B electron microscope operating at 200 kV (C_s = 0.4 mm). The microscopes are equipped with KEVEX analyzers. For each of the samples, energy dispersive spectroscopy (EDS) analyses were systematically carried out on numerous grains.

The X-ray powder diffraction (XRD) data were collected, at room temperature (RT), with a Philips diffractometer (Cu Kα radiation) in the range 10° $\leq 2\theta \leq$ 100° by increment of 0.02° (2θ). The oxygen content was measured by chemical titration.

The resistivity measurements were performed from room temperature down to 5 K, by the four-probe method on sintered bars, in the earth magnetic field or in 7 T. The magnetization versus temperature was registered on warming with a vibrating sample magnetometer or in a SQUID magnetometer in a magnetic field of 1.4 T, which was applied at 4.2 K after a zero field cooling.

Results and Discussion

X-ray Diffraction and Chemical Analysis. The EDS analyses of the different samples show that the cationic composition of the crystallites is identical to the nominal one in the limits of the errors, regardless of the synthesis conditions. The oxygen content determined by iodometric titration, and the room temperature cell parameters refined from X-ray data (Figure 1) are summarized in Table 1. The comparison of the x = 0.9 samples shows that the "air" sample exhibits a practically "O_3" stoichiometry but is biphasic (Figure 1a), consisting of a distorted orthorhombic perovskite as a major phase and the hexagonal perovskite as a secondary one. By heating this "air" $Pr_{0.1}Sr_{0.9}MnO_3$ compound in argon, one obtains an oxygen-deficient perovskite "air+Ar" $Pr_{0.1}Sr_{0.9}MnO_{2.71}$. Remarkably, the latter is cubic, without any traces of the hexagonal perovskite (Figure 1b). The annealing of the "air+Ar" $Pr_{0.1}Sr_{0.9}MnO_{2.71}$ perovskite under oxygen pressure leads to a second pure cubic and stoichiometric perovskite (Figure 1c), "air+Ar+O_2" $Pr_{0.1}Sr_{0.9}MnO_3$, whose a parameter is significantly smaller than the "air+Ar" $Pr_{0.1}Sr_{0.9}MnO_{2.71}$ phase, in agreement with the oxidation of Mn^{3+} into Mn^{4+}. These observations show that the synthesis in an argon atmosphere, leading to an oxygen-deficient perovskite, is the clue to avoid the formation of the hexagonal perovskite. Then the perovskite close to O_3 stoichiometry can be obtained by annealing the latter at lower temperature under oxygen pressure.

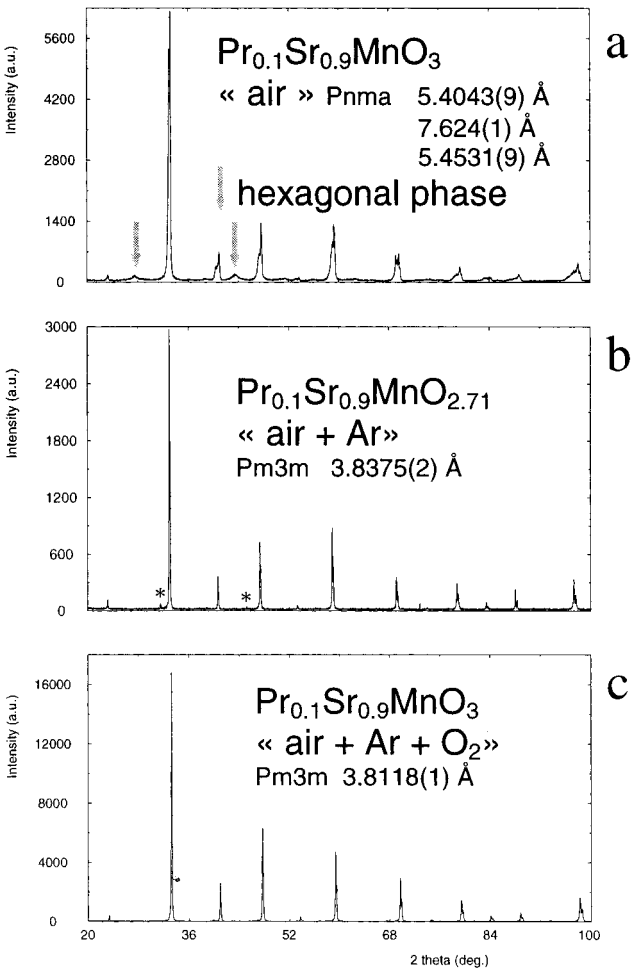

Figure 1. $Pr_{0.1}Sr_{0.9}MnO_{3-\delta}$: X-ray patterns of the "air" (a), "air+Ar" (b), and "air+Ar+O_2" (c) samples. In part a, the arrows indicate the reflections due to the hexagonal phase and in part b, the stars are for the weak reflections of the oxygen deficient supercells.

Table 1. $Pr_{1-x}Sr_xMnO_{3-\delta}$: Influence of the Synthesis on the Crystallographic Parameters

x	reference	δ[a]	space group	cell parameters (Å)
0.90	"air"	0.01(2)	P type "defective structure"	5.4043(9)[b] 7.6245(2)[b] 5.4531(9)[b]
	"air+Ar"	0.29(2)	*Pm*3*m*	3.8375(2)
	"air+Ar+O_2"	0.01(2)	*Pm*3*m*	3.8118(1)
0.95	"air+Ar+O_2"	0.08(2)	*Pm*3*m*	3.8091(1)
1	"air+Ar+O_2"	0.08(2)	*Pm*3*m*	3.8056(1)

[a] Average oxygen content determined by iodometric titration. [b] Average parameters of the main orthorhombic perovskite phase.

(12) Maignan, A.; Martin, C.; Damay, F.; Raveau, B. *Chem. Mater.* **1998**, *10*, 950.

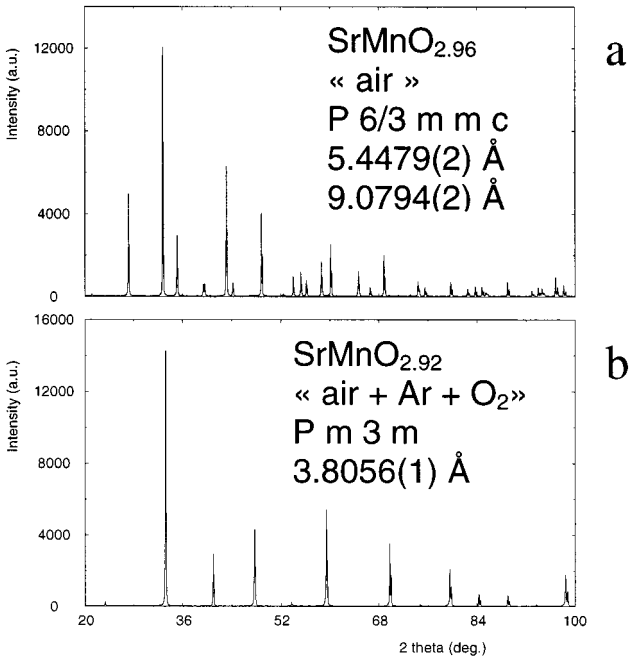

Figure 2. $SrMnO_{3-\delta}$: X-ray patterns of the "air" and "air+Ar+O_2" samples.

The difficulty of obtaining a cubic stoichiometric perovskite increases with x, i.e., approching pure $SrMnO_3$. For $x = 0.95$, a cubic perovskite can still be obtained by annealing the "air+Ar" phase under oxygen pressure. However, one observes an oxygen deficiency, leading to the formula $Pr_{0.05}Sr_{0.95}MnO_{2.92}$ for the "air+Ar+O_2" sample (Table 1). Similarly, for $x = 1$, the "air" $SrMnO_{2.96}$ compound corresponds to the hexagonal form (Figure 2a), whereas the "air+Ar+O_2" phase $SrMnO_{2.92}$ is an oxygen-deficient cubic perovskite (Figure 2b).

Electron Microscopy Study. *The "Air" Samples: A Continuous Intergrowth between the Cubic and the Hexagonal Structures.* The ED investigation of the "air" $Pr_{0.10}Sr_{0.90}MnO_3$ evidences a very defective structure, showing that the distorted cell obtained from XRD data corresponds in fact to an average structure. To understand this behavior, a comparison with the cubic perovskite $Pr_{0.15}Sr_{0.85}MnO_3$ previously studied[2] is necessary. In contrast to the ED patterns and to the [110] HREM image of $Pr_{0.85}Sr_{0.15}MnO_3$ (Figure 3), which are characteristic of a pure cubic perovskite, the ED patterns of the "air" $Pr_{0.10}Sr_{0.90}MnO_3$ sample are complex (Figure 4c). Besides the intense reflections of the cubic cell, they show additional weak and streaked reflections belonging to different stacking sequences. The distance between the origin and the 111_c reflection is subdivided into six equal parts, i.e., the period along this reciprocal direction is of the order of 13 Å. This points toward a 6L (or 12L) structure. The low magnification (Figure 4a) and HREM (Figure 4b) images confirm this viewpoint: the crystals consist of large cubic domains intergrown with hexagonal 6L small domains or isolated 6L extended defects parallel to the $\{111\}_c$ perovskite plane.

Decreasing the Pr content, i.e., increasing x up to 0.95, the 6L (or 12L) polytype structure becomes majority. Figure 5 shows an almost perfect structure; the corresponding diffraction pattern shows elongated reflections, but the intense cubic reflections have disappeared and

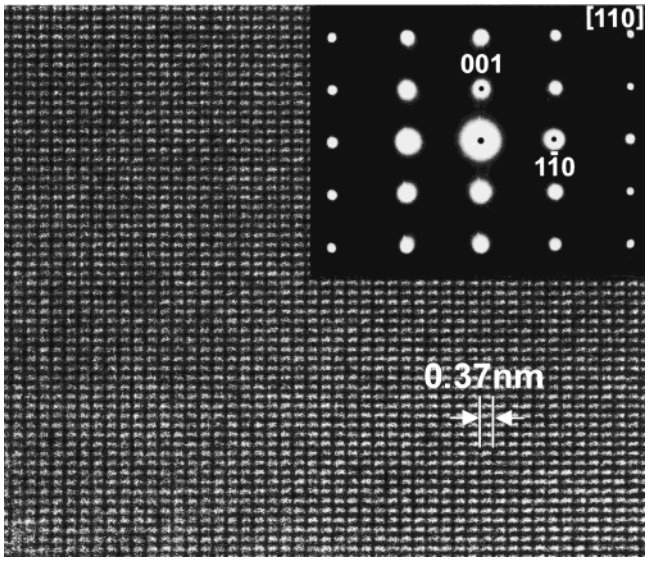

Figure 3. [110] ED pattern and HREM image of a perfect cubic perovskite phase ($x = 0.85$).

the hexagonal periodicity is clearly visible. The HREM images also show that the structure is subunit cell twinned, similar to previous hexagonal perovskite systems.[13−14] Finally for $x = 1$, the regular 4L structure is obtained. These results demonstrate that there exists a possibility of disordered intergrowths of the cubic and hexagonal variants of the perovskite in a continuous way as x varies from 0.85 to 1.

The "Air+Ar" Cubic Oxygen-Deficient Perovskite $Pr_{0.10}Sr_{0.90}MnO_{2.71}$. As mentioned above, the "air+Ar" sample is oxygen-deficient, namely $Pr_{0.1}Sr_{0.9}MnO_{2.71}$. The most important result of the electron diffraction and HREM studies of this "air+Ar" sample deals with the fact that all stacking faults have disappeared; there are no further traces of hexagonal structure. The patterns and the HREM images are similar to those of $Pr_{0.15}Sr_{0.85}MnO_3$ (Figure 3), indicative of a cubic perovskite phase.

Note that the direct synthesis of the $x = 0.9$ sample in argon leads to much larger oxygen deficiency, so that the obtained phase, $Pr_{0.10}Sr_{0.90}MnO_{2.55}$, contains only Mn^{3+}. The ED investigation of this "Ar" sample confirms that the hexagonal phases and polytypes are not formed under such oxygen free atmosphere. However, one observes that the crystallites of cubic perovskite type, observed in the "air+Ar" sample, are now a minority. Most of the grains consist of a mosaic texture of two types of oriented domains which correspond to two types of superstructures. The first one is tetragonal with $a \approx a_p\sqrt{5}$ and $c \approx a_p$ and the second is orthorhombic with $a \approx a_p 2\sqrt{2}$, $b \approx a_p\sqrt{2}$, and $c \approx a_p$. These two structural types can be interpreted by an ordering between the oxygen vacancies and the oxygen atoms. They were described earlier in $CaMnO_{3-\delta}$[15,17] and $SrMnO_{2.5}$.[18]

(13) Shpanchenko, R. V.; Nistor, L.; Van Tendeloo, G.; Van Landuyt, J.; Amelinckx, S. A.; Abakumov, A. M.; Antipov, E. V.; Kouba, L. M. *J. Solid State Chem*. **1995,** *114*, 560.
(14) Shpanchenko, R. V.; Abakumov, A. M.; Antipov, E. V.; Nistor, L.; Van Tendeloo, G.; Amelinckx, S. A. *J. Solid State Chem*. **1995**, *118*, 180.
(15) Reller, A.; Thomas, J. M.; Jefferson, D. A.; Uppal, M. K. *Proc. R. Soc. London A* **1984**, *394*, 223.
(16) Poeppelmeier, K. R.; Leonowicz, M. E.; Longo, J. M. *J. Solid State Chem*. **1982**, *44*, 89.

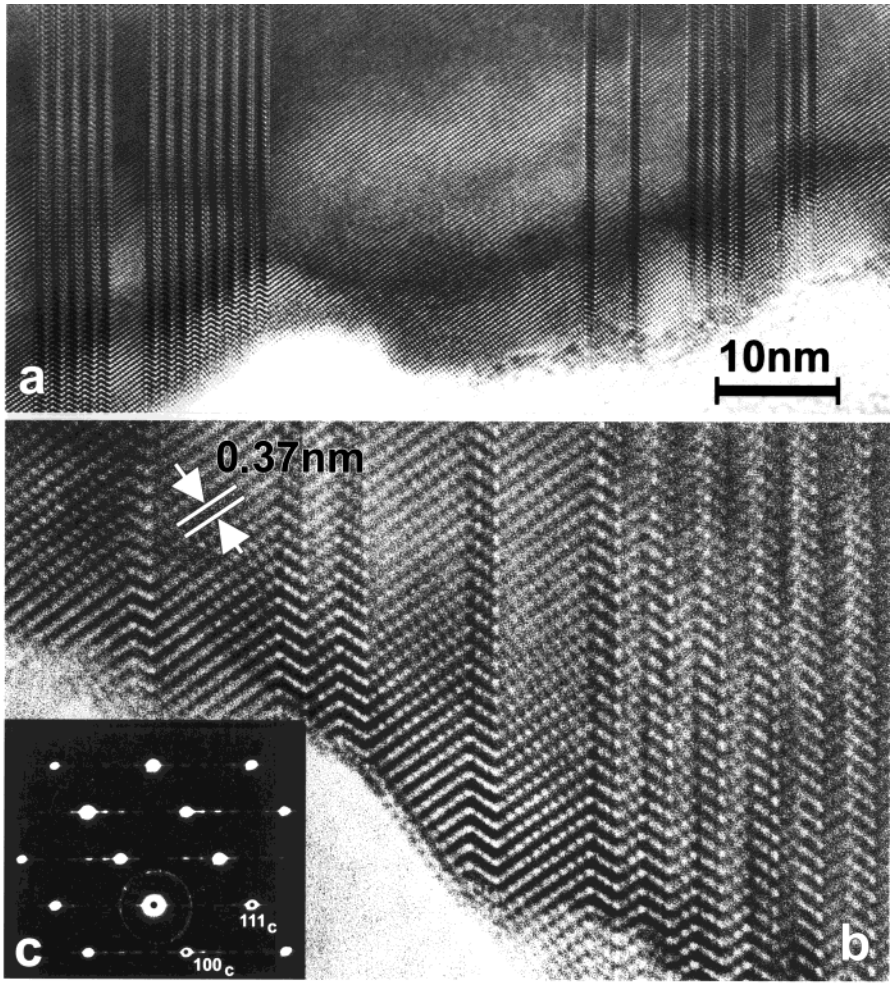

Figure 4. "air" $Pr_{0.1}Sr_{0.9}MnO_3$. Examples of low magnification images showing wide cubic areas (a) and isolated 6L defects (b). The ED patterns (c) exhibit weak and streaked reflections along $[111]_p$.

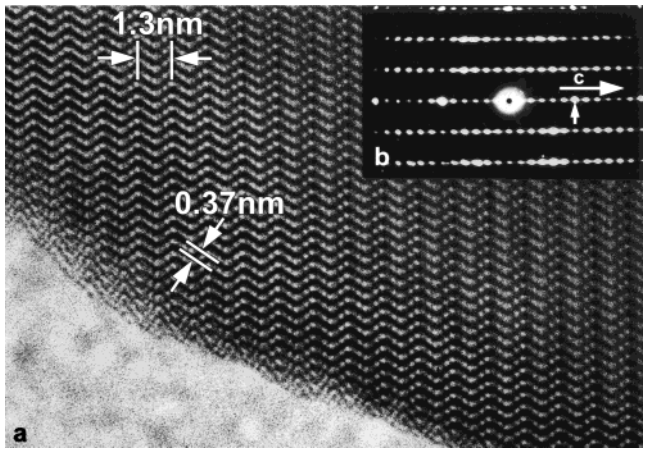

Figure 5. "air" $Pr_{0.05}Sr_{0.95}MnO_3$: (a) HREM image and (b) ED pattern. The 6L structure is favored.

The "Air+Ar+O_2" Cubic Perovskite $Pr_{0.10}Sr_{0.90}MnO_3$. The ED pattern and HREM image of this "air+Ar+O_2" phase registered at room temperature are identical to those previously observed for the cubic perovskite $Pr_{0.15}Sr_{0.85}MnO_3$,[2] in agreement with its X-ray pattern (Figure 1c). This demonstrates the great homogeneity and a good crystallization of the cubic stoichiometric perovskite, the hexagonal defects being not restored by annealing under an oxygen pressure at low temperature (600 °C).

Such a stoichiometric perovskite is of interest for magnetic and transport properties, since it exhibits, like $Pr_{0.15}Sr_{0.85}MnO_3$, a cubic symmetry. For this reason, its ED pattern was registered versus temperature.

At 92 K, the reconstruction of the reciprocal space evidences a structural change. One observes a tetragonal supercell with $a \approx a_p\sqrt{2}$ and $c \approx 2a_p$. The conditions limiting the reflection are consistent with an *I*4/*mcm* space group. The [100], [111], and [010] patterns are given in Figure 6. Such a superstructure is generated by a distortion of the cubic perovskite cell $a^0a^0c^-$ following the Glazer notation.[19] The crystallites systematically exhibit twinning domains. These domains are commonly observed in such distorted perovskite structure since the distortion arises along the equivalent directions of the perovskite subcell. An example of twinning domains is given in Figure 7a; the bright field image is recorded at 92 K.

When the crystallites are warmed, the distortion and twinning domains disappear at about $T \approx 180$ K. The transition is reversible. A bright field image of the above area is given in Figure 7b, recorded at 185 K. It shows that the sample is now twin free.

(17) Poeppelmeier, K. R.; Leonowicz, M. E.; Scanlon, J. S.; Longo, J. M. *J. Solid State Chem.* **1982**, *45*, 71.
(18) Caignaert, V. *J. Magn. Magn. Mater.* **1997**, *116*, 117.
(19) Glazer, A. M. *Acta Crystallogr.* **1972**, *B28*, 3384.

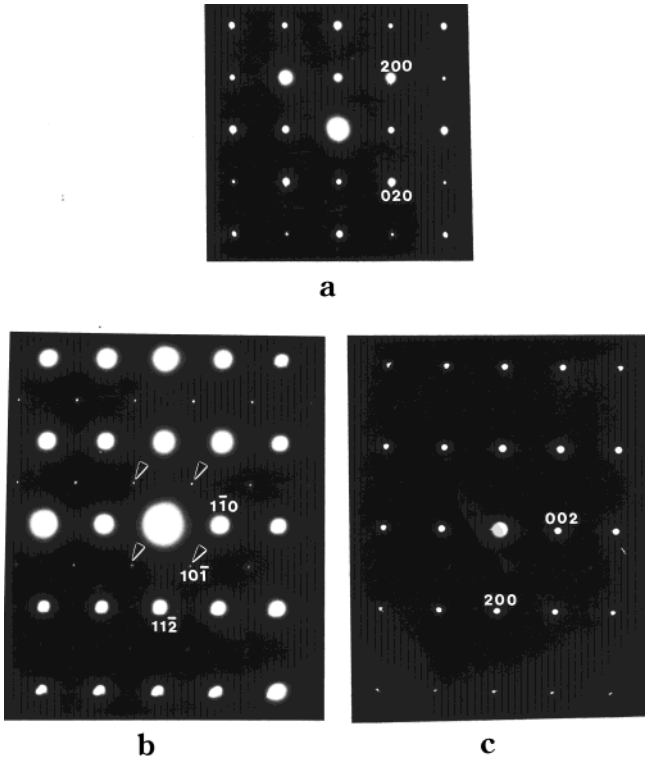

Figure 6. "air+Ar+O_2" $Pr_{0.1}Sr_{0.9}MnO_3$: (a) [110], (b) [111], and (c) [010] ED patterns recorded at 92 K. They evidence a *I*4/*mcm*-type structure.

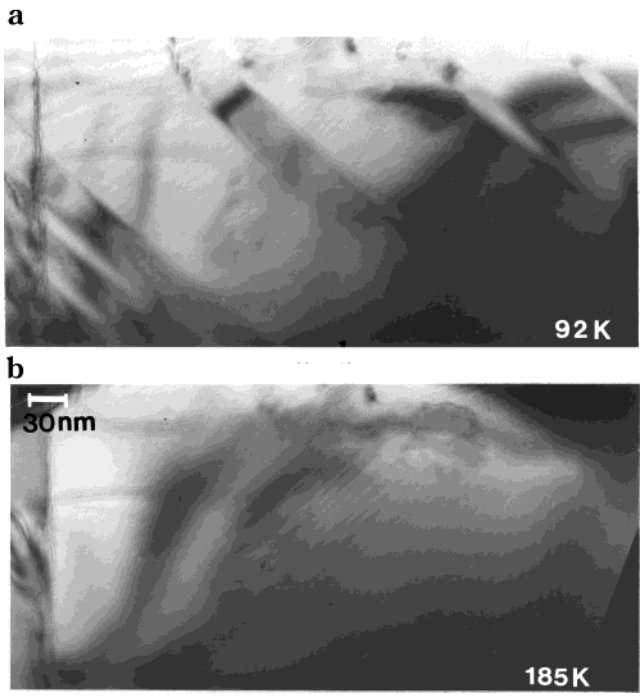

Figure 7. "air+Ar+O_2" $Pr_{0.1}Sr_{0.9}MnO_3$: bright field images recorded at (a) 92 K and (b) 185 K, i.e., below and above the transition temperature.

Magnetization and Transport Properties. The complexity of the magnetic properties of the $Pr_{1-x}Sr_xMnO_{3-\delta}$ samples in the range $0.85 \leq x \leq 1$ depending on the structural type is illustrated by the final member, $SrMnO_3$. For the hexagonal forms of $SrMnO_3$, it was shown that the 4L and 6L polytypes exhibit different curves of susceptibility as a function of temperature with a χ maximum at ~350 K, indicative of some

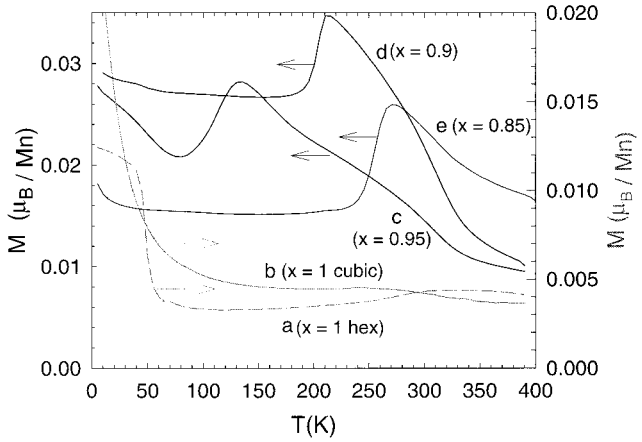

Figure 8. Temperature dependence of the magnetization (zfc, 1.45*T*) for the hexagonal (a) and cubic (b) forms of $SrMnO_{3-\delta}$ and for the cubic perovskites $Pr_{0.05}Sr_{0.95}MnO_{2.92}$ (c), $Pr_{0.10}Sr_{0.90}MnO_3$ (d), and $Pr_{0.15}Sr_{0.85}MnO_3$ (e).

antiferromagnetism for the former, whereas a parasitic ferromagnetism below 90 K was revealed in the latter.[20] However, the negative intercepts of the $\chi^{-1}(T)$ curves with the *T* axis are indicative of antiferromagnetism. More recently, the magnetism of the phase 4L-$SrMnO_3$ was reinvestigated by Mössbauer spectroscopy.[8] Though a χ maximum was also observed at ~350 K, the antiferromagnetic ordering temperature was found to be $T_N \sim 280$ K. The apparent discrepancy between $\chi(T)$ curve and Mössbauer data was explained by considering the short-range antiferromagnetism of Mn_2O_9 clusters to be responsible for the χ maximum at ~350 K. Finally, the magnetic structure of the cubic type of $SrMnO_3$ was also reported.[7] Cubic $SrMnO_3$, prepared by annealing the oxygen-deficient $SrMnO_{2.5}$, is a G-type antiferromagnet with $T_N = 260$ K, a temperature which is in good agreement with the χ maximum at the same temperature. Our results obtained for the "air" hexagonal perovskite $SrMnO_{2.96}$ and for the "air+Ar+O_2" cubic perovskite $SrMnO_{2.92}$ corroborate the previous studies. The *M*(*T*) curves of these two compounds (Figure 8) exhibit a maximum at 330 and 260 K for hexagonal $SrMnO_{2.96}$ and cubic $SrMnO_{2.92}$, respectively. Thus, we assume that cubic perovskite $SrMnO_{2.92}$ is a G-type antiferromagnet with $T_N \approx 260$ K. The cubic phase ($SrMnO_{2.92}$) is quasimetallic from 300 K to 100 K ($\rho_{300K} \approx 0.5\ \Omega$ cm) (Figure 9, curve b), like the AFM cubic $SrFeO_3$ perovskite,[21] whereas the hexagonal form is a semiconductor (Figure 9, curve a), with a resistivity of several orders of magnitude larger at 300 K. This metallicity of the cubic perovskite $SrMnO_{2.92}$ originates not only from its larger electron doping but also from its 180° Mn−O−Mn exchange pathways.

This first set of magnetization and transport data demonstrates the influence of the structural type for the physical properties. It is confirmed by the fact that the "air" $Pr_{0.10}Sr_{0.90}MnO_3$ distorted perovskite containing some intergrowths of hexagonal variants is a semiconductor (Figure 9, curve c) with a much higher resistivity than the "air+Ar+O_2" cubic $Pr_{0.10}Sr_{0.90}MnO_3$ (Figure 9, curve d). Thus, it is more reasonable to compare samples

(20) Chamberland, B. L.; Sleight, A. W.; Weiher. J. F. *J. Solid State Chem.* **1970**, *1*, 506.
(21) Takeda T.; Yamaguchi Y.; Watanabe H. *J. Phys. Soc. Jpn.* **1972**, *33*, 967.

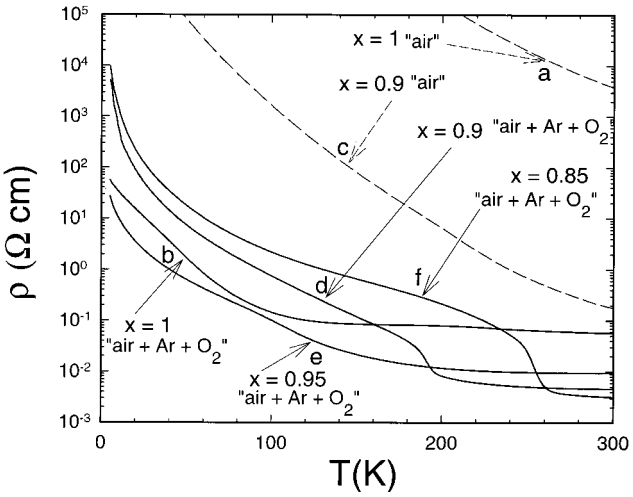

Figure 9. Temperature dependence of the resistivity (under 0 and 7 T) for the hexagonal (a) and cubic (b) $SrMnO_{3-\delta}$ samples, for the "air" (c) and "air+Ar+O_2" (d) $Pr_{0.1}Sr_{0.9}MnO_3$ compounds and for the cubic $Pr_{0.05}Sr_{0.95}MnO_{2.92}$ (e) and $Pr_{0.15}Sr_{0.85}MnO_3$ (f) perovskites.

crystallizing in the same cubic structure, i.e., "air+Ar+O_2" samples and also $Pr_{0.15}Sr_{0.85}MnO_3$ (previously prepared[2]). Comparing the "air+Ar+O_2" cubic perovskites $SrMnO_{2.92}$ (Figure 9, curve b), $Pr_{0.05}Sr_{0.95}MnO_{2.92}$ (Figure 9, curve e), $Pr_{0.10}Sr_{0.90}MnO_3$ (Figure 9, curve d), and $Pr_{0.15}Sr_{0.85}MnO_3$ (Figure 9, curve f), one observes that the resistivity at room temperature is higher for $SrMnO_{2.92}$ and for $Pr_{0.05}Sr_{0.95}MnO_{2.92}$ (curves b and e) than for the other samples $Pr_{0.10}Sr_{0.90}MnO_3$ and $Pr_{0.15}Sr_{0.85}MnO_3$ (curves d and f), despite their larger carrier concentration. Such a behavior due to oxygen deficiency shows that the extra electrons are localized by the potential of oxygen vacancies and do not contribute to the conduction. But, more important is the existence of a jump of resistivity around 200 and 270 K for $Pr_{0.10}Sr_{0.90}MnO_3$ (curve d) and for $Pr_{0.15}Sr_{0.85}MnO_3$ (curve f), respectively. The present observations versus temperature and previous ones on $Pr_{0.15}Sr_{0.85}MnO_3$ suggest that these resistivity jumps are associated with a structural transition from the cubic to the tetragonal $I4/mcm$ symmetry as T decreases. This structural transition was in fact shown to be coupled with a paramagnetic to C-type antiferromagnetic transition at $T_N \approx 270$ K for $Pr_{0.15}Sr_{0.85}MnO_3$.[2] The recent NPD study of the cubic $Pr_{0.10}Sr_{0.90}MnO_3$ compound confirms this statement:[22] this phase exhibits indeed an AFM structure at low temperature which appears at $T_N \approx 200$ K, i.e., connected with the structural transition. Thus, the structural distortion at T_N is responsible for the resistivity jump at 200 and 270 K for the $Pr_{0.10}$- and $Pr_{0.15}$-doped manganites, respectively. The inflection on the $\rho(T)$ curve of the $Pr_{0.05}$-doped sample, around 130 K (curve e), suggests that this phenomenon begins already to appear for $x = 0.05$.

The $M(T)$ curves of these cubic perovskites (Figure 8) show a magnetization drop at 270, 200, and 130 K for $Pr_{0.15}Sr_{0.85}MnO_3$ (curve e), $Pr_{0.10}Sr_{0.90}MnO_3$ (curve d), and $Pr_{0.05}Sr_{0.95}MnO_{2.92}$ (curve c), respectively, in perfect agreement with the resistivity curves. Thus, the Pr-doping induces a coupled structural−magnetic transition, T_N from the $M(T)$ curves increasing with the Pr content from 130 K for $x = 0.05$ to 270 K for $x = 0.15$. To date, the AFM-type of these compounds at low temperature (4.2 K) is not completely elucidated. Nevertheless, from the preliminary NPD study, it appears clearly that starting from a G-type AFM phase at low temperature a second C-type AFM structure appears by Pr-doping, so that for the "air+Ar+O_2" $Pr_{0.05}Sr_{0.95}MnO_3$ and $Pr_{0.10}Sr_{0.90}MnO_3$ both C and G-type coexist,[22] and finally for $Pr_{0.15}Sr_{0.85}MnO_3$, the C type is obtained alone.[2] The ND patterns registered at 2 K, using the G41 diffractometer (in LLB, Saclay, France), are given in Figure 10, to illustrate this evolution of the magnetic structures with x in the $Pr_{1-x}Sr_xMnO_3$ series. Thus, the C-type AFM structure should be responsible for the appearance of the coupled structural/magnetic/resistive transition. The absence of structural distortion and of resistivity jump for the cubic $SrMnO_{2.92}$, which is

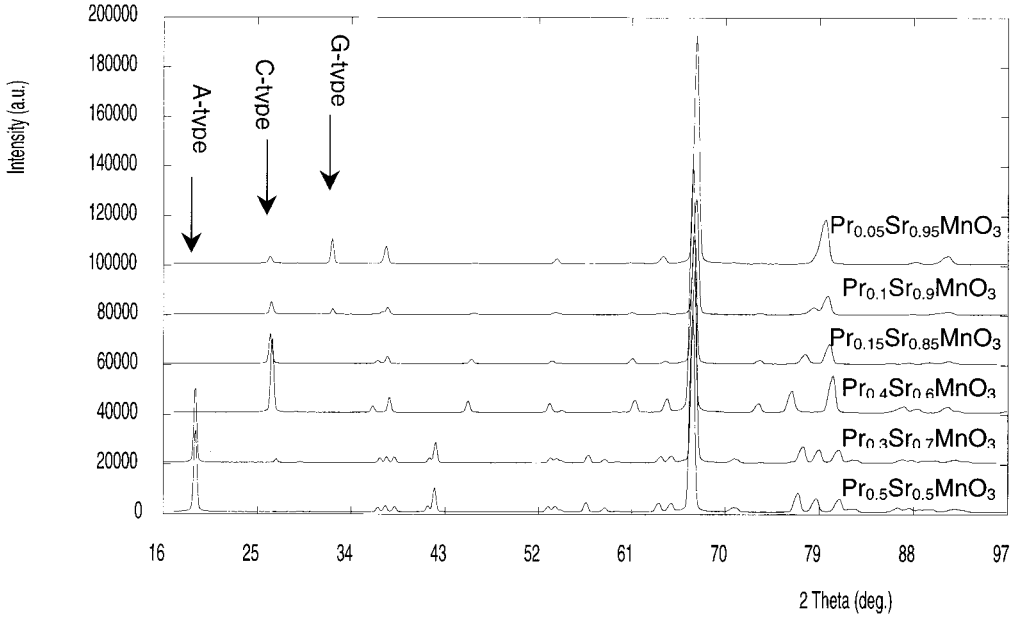

Figure 10. Neutron diffraction patterns, recorded at 2 K with $\lambda = 2.4266$ Å, for few compositions, labeled on the graph, in the $Pr_{1-x}Sr_xMnO_3$ series. The low-angle reflections characteristic of the A-, C-, and G-type AFM structures are indicated.

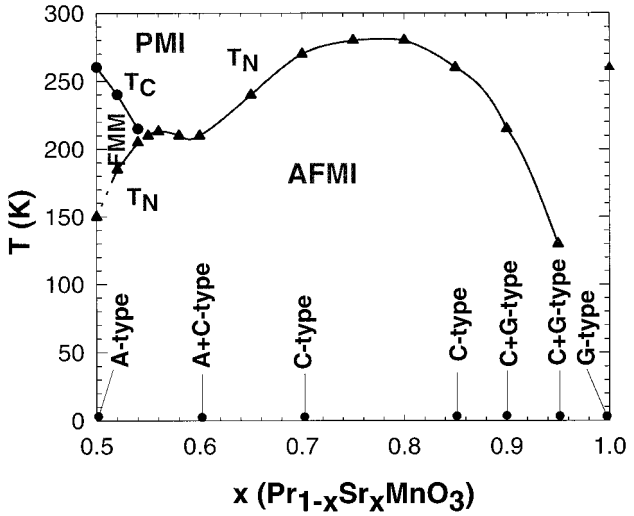

Figure 11. Mn^{4+}-rich part of the phase diagram $Pr_{1-x}Sr_xMnO_3$. The AF type reported have been determined by NPD at low temperature for the few compositions from Figure 10, except for $SrMnO_3$ which is from ref 7.

believed to be a G-type AFM phase as $SrMnO_3$,[7] supports also this viewpoint. It is also this absence of distortion at the AFM transition of the G-type phase which explains that the semimetallic behavior of cubic $SrMnO_{2.92}$ covers a larger range of temperature, down to 130 K than the Pr-doped cubic perovskites, despite its higher resistivity.

Finally, the possibility to synthesize and characterize Mn^{4+}-rich manganites $Pr_{1-x}Sr_xMnO_3$ with a cubic symmetry allows the magnetic phase diagram of this system[3] to be completed, in the Mn^{4+} region $0.85 < x \leq 1$ (Figure 11). The T_C and T_N values reported on this diagram have been extracted from the magnetization curves. The T_N minimum observed for $x = 0.95$ is connected with the decrease of the C-type AFM interactions. The important characteristic of this part of the diagram deals with the coexistence at low temperature of C and G-type AFM phases for $0.9 \leq x < 1$. This coexistence of C and G-types AFM is also observed in the Mn^{4+}-rich compounds $Ln_{1-x}Ca_xMnO_3$, as exemplified for $Sm_{0.15}Ca_{0.85}MnO_3$.[2] But for these calcium samples, around $x \approx 0.9$, the G-type AFM phase goes with a FM component.[22] The absence of competition between metallic FM and insulating AFM in the Mn^{4+}-rich $Pr_{1-x}Sr_xMnO_3$ perovskites explains their inability to yield CMR properties.

Acknowledgment. The authors thank the University of Caen for supporting this work through a position of associate Professor.

CM000016O

(22) Martin, C.; Maignan, A.; Hervieu, M.; Raveau, B.; Jirák, Z.; Savosta, M. M.; Kurbakov, A.; Trounov, V.; André, G.; Bourée, F. Manuscript in preparation.